Spin excitations in the low-temperature phase of Tm

S. H. Liu
Department of Physics, University of California, San Diego, La Jolla, California 92093-0319
(Received 5 February 1996; revised manuscript received 25 March 1996)

The rare-earth metal thulium has the ferrimagnetic-antiphase-domain spin arrangement at low temperatures. We show that the spin excitations in this magnetic structure are nearly localized and largely dispersionless modes. There are seven such modes between 8 and 10 meV, and they have not been resolved by neutron scattering experiments. On the other hand, these modes have different neutron scattering cross sections in different magnetic superzones, and this gives rise to what appears as a dispersion in the spin excitation peak in the extended Brillouin zone of the crystal. [S0163-1829(96)09033-9]

I. INTRODUCTION

The heavy rare-earth element thulium (Tm) has the hexagonal-close-packed (hcp) crystal structure. It orders antiferromagnetically below 54 K in a sinusoidal spin structure in which the atomic moments in the same hexagonal plane are aligned parallel to one another along the crystal *c* axis, and the net moments on different planes form a sinusoidal distribution.[1–5] There is no net ordered moment. The periodicity of the structure, slightly larger than seven layers, is incommensurate with the lattice. At a lower temperature, roughly 40 K, the sinusoidal structure begins to square up by developing a third harmonic, then a fifth harmonic, etc.[6] In the meantime, the period of the structure decreases linearly toward seven layers as the temperature is decreased. At 32 K a first order phase transition occurs such that the magnetic structure becomes commensurate with the crystal structure. The spin structure has a repeat distance of exactly seven layers, with the spins in four adjacent layers pointing up the *c* axis and those in the other three adjacent layers pointing down. The imbalance of spins in the up and down sublattices produces a net ferrimagnetic moment.

The magnetic excitations in the ferrimagnetic phase of Tm have been observed by two independent groups.[6–9] We summarize the results briefly as follows: In the low energy range, below 8 meV, at least three branches of acoustic modes have been observed. These modes emerge from magnetic satellite points and have the dispersion curves that are close to that of transverse acoustic (TA) phonons. There has been some debate about the origin of these modes. Fernandez-Baca *et al.*[8,9] identified these modes as originating from magnetovibrational scattering, i.e., TA phonons generated by the interaction between the scattered neutrons and the localized magnetic moments, but McEwen *et al.*[6,7,10] have argued that dynamical phonon-magnon coupling plays the dominant role. In the high energy range, between 8 and 10 meV, a branch of spin excitations have been seen. The branch shows weak dispersion when plotted in the extended zone of the hcp structure, and has the energy very close the separation between the two lowest crystal field levels in Tm.[11]

In Ref. 7 McEwen *et al.* presented a formal discussion of the magnetic excitations in complex magnetic structures such as Tm. The authors formulated a generalized random-phase approximation for finite temperatures, including the interaction between phonons and spin waves, using a model which contains long-range exchange coupling and full crystal field interactions. They pointed out all of the complications that arose due to the seven layer structure of Tm, and showed a complete calculation of the mixed magnon-phonon dispersion curves. For the high energy modes, however, they only displayed the results of a hypothetical ferromagnetic structure. Because the calculation was handled numerically, they did not elaborate on the analytical properties of the spin excitations. The purpose of this paper is to fill this gap. We will limit our analysis by using a phenomenological Hamiltonian which ignores the phonon-magnon coupling. We will show that the ferrimagnetic spin excitations have unique properties that make them very different from ferromagnetic excitations, and we compare the result of our calculation with experiments.

To summarize our results, we find that the spin excitations are nearly local modes with little dispersion. There are seven practically flat branches in every magnetic superzone, which is one-seventh of the extended zone of the hcp crystal. The branches cannot be folded out into the extended zone. The branches have different neutron scattering cross-sections in different magnetic superzones. With imperfect resolution the spin excitation branch has the appearance of dispersion in the extended zone of the crystal, as found experimentally.

In the next section we formulate and solve the spin excitation problem in the ferrimagnetic structure. In Sec. III we calculate the neutron scattering cross section of the magnetic excitations and show that it explains adequately the experimental findings. Section IV formulates the same problem in the momentum space. This method has the advantage that the cross section can be obtained more directly.

II. SPIN EXCITATIONS IN THE FERRIMAGNETIC PHASE

We adopt the simplest possible phenomenological Hamiltonian for the system:

$$H=-\sum_{i,j} J_{ij}\mathbf{S}_i\cdot\mathbf{S}_j-K\sum_i (S_i^z)^2, \tag{1}$$

where J_{ij} denotes the long-range exchange coupling between two spins at sites labeled by i and j, and K is the single site twofold anisotropy constant. It has been shown that the sinusoidal spin structure just below the Néel temperature is formed provided that the exchange interaction favors a periodic spin structure and the magnetic anisotropy favors spin alignments along the crystal c axis.[12] One defines the Fourier transform of J_{ij} by

$$\mathcal{J}(\mathbf{q})=\sum_j J_{ij}e^{i\mathbf{q}\cdot\mathbf{R}_{ij}}, \tag{2}$$

where $\mathbf{R}_{ij}$ is the vector distances between the sites i and j. A periodic spin structure is energetically favored if $\mathcal{J}(\mathbf{q})$ is a maximum at $\mathbf{q}=\mathbf{Q}\neq 0$. In Tm the vector $\mathbf{Q}$ is along the c axis, and at low temperatures the length of $\mathbf{Q}$ is $Q=4\pi/7c$. The anisotropy constant K embodies both the crystal field contribution and the magnetoelastic contribution. We choose to work with this phenomenological Hamiltonian in order to keep the formulation at the simplest possible level. The physical conclusions reached in this work are independent of the model Hamiltonian.

We further divide the crystal into magnetic cells, each containing seven hexagonal layers, and label them by the cell index l. Within each cell, four layers labeled by $n=1$–4 have their net moments in the positive z direction, and three layers with $n=5$–7 have net moments in the negative z direction. A spin excitation may be generated by the operator $S_i^+=S_i^x+iS_i^y$ or its Hermitian conjugate S_i^-. The equation of motion for the former is

$$\omega S_i^+=[S_i^+,H]=2\sum_j J_{ij}(S_i^+S_j^z-S_i^zS_j^+)+2KS_i^+S_i^z. \tag{3}$$

The right-hand side of Eq. (3) is linearized by factoring out the ordered moment $\langle S_j^z\rangle=\pm S$. The result of this step is most easily written down in terms of plane wave amplitudes $A_n(q)$. We restrict the vector $\mathbf{q}$ along the c axis, i.e., $\mathbf{q}=(0,0,q)$, and define

$$S_i^+=a_n(q)e^{7iqlc/2}, \tag{4}$$

where l is the unit cell containing the site i, n is the layer containing i. It is also useful to define a set of contracted exchange interaction in the ferrimagnetic structure by

$$J_m=\sum_{j\in n+m} J_{ij}, \tag{5}$$

where the sum on j is over all sites in the layer which is m layers away from the site i. For convenience we cut off the exchange interaction at $m=6$, because this already includes more parameters than one can hope to extract from the data. The contracted exchange parameters are related to the Fourier transform $\mathcal{J}(\mathbf{q})$ by

$$\mathcal{J}(\mathbf{q})=J_0+2\sum_m J_m\cos(mqc/2). \tag{6}$$

In terms of these new symbols the linearized equations of motion are

$$\omega A_n(q)=\sum_{n'=1}^{7} M_{nn'}A_{n'}(q), \tag{7}$$

where the 7×7 dynamical matrix for the spin excitations has the form

$$\tilde{M}=\begin{pmatrix}
M_{11} & M_{12} & M_{13} & M_{14} & M_{15} & M_{16} & M_{17}\\
M_{12}^* & M_{22} & M_{12} & M_{13} & M_{14} & M_{15} & M_{16}\\
M_{13}^* & M_{12}^* & M_{22} & M_{12} & M_{13} & M_{14} & M_{15}\\
M_{14}^* & M_{13}^* & M_{12}^* & M_{11} & M_{12} & M_{13} & M_{14}\\
-M_{15}^* & -M_{14}^* & -M_{13}^* & -M_{12}^* & -M_{55} & -M_{12} & -M_{13}\\
-M_{16}^* & -M_{15}^* & -M_{14}^* & -M_{13}^* & -M_{12}^* & -M_{66} & -M_{12}\\
-M_{17}^* & -M_{16}^* & -M_{15}^* & -M_{14}^* & -M_{13}^* & -M_{12}^* & -M_{55}
\end{pmatrix}, \tag{8}$$

where

$$M_{11}=2SK,$$

$$M_{22}=2S[K+J_1-J_3-J_4+J_6],$$

$$M_{55}=2S[K-J_3-J_4],$$

$$M_{66}=2S[K+J_1-J_2-J_3-J_4-J_5+J_6],$$

$$M_{1n}=-2S[J_{n-1}+J_{8-n}e^{-i7qc/2}], \tag{9}$$

for $n=2$–7. The eigenvalues of the matrix $\tilde{M}$ gives the energies of the spin excitation modes. The negative signs in the last three rows in Eq. (8) result from the fact that in the layers $n=5$–7 the ordered moments point in the negative z direction.

We can extract a considerable amount of qualitative information about the spin excitations without elaborate algebra. In the limit that $K\gg J_m$, the excitation energies are $\pm 2SK$, where the upper sign is fourfold degenerate and the lower sign is threefold-degenerate. These are all localized modes in the up and down sublattices, respectively, and the negative sign of the last three energies arises from the fact that the operator S_i^+ actually creates spin deviations in the down sublattice. For finite but weak J's, as in Tm, we obtain good approximations for the energies by diagonalizing the 4×4 and 3×3 blocks for the two sublattices separately, be-

cause the anisotropy energy acts like strong potential barriers which confine the spin excitations in their respective sublattices. Consider the case $q=0$ or $2\pi/7c$ for which the matrix is real. It is easily seen from the symmetry of the matrix elements that the eigenvectors are of the form

$$(\tilde{A}(q))^{\dagger}=(\alpha,\beta,\beta,\alpha)$$

and

$$(\tilde{A}(q))^{\dagger}=(\alpha,\beta,-\beta,-\alpha), \tag{10}$$

for the up sublattice $n=1$–4, and

$$(\tilde{A}(q))^{\dagger}=(\gamma,\delta,\gamma)$$

and

$$(\tilde{A}(q))^{\dagger}=(\gamma,0,-\gamma), \tag{11}$$

for the down sublattice $n=5$–7. The corresponding eigenvalues are

$$\omega=\frac{1}{2}\{M_{11}+M_{22}+M_{12}+M_{14}\pm[(M_{11}-M_{22}-M_{12}+M_{14})^2+4(M_{12}+M_{13})^2]^{1/2}\},$$

$$\omega=\frac{1}{2}\{M_{11}+M_{22}-M_{12}-M_{14}\pm[(M_{11}-M_{22}+M_{12}-M_{14})^2+4(M_{12}-M_{13})^2]^{1/2}\},$$

for the four local modes in the up sublattice. These energies are labeled ω_k with $k=1$–4 in the ascending order. The three modes in the down sublattice have the eigenvalues

$$\omega=-\frac{1}{2}\{M_{55}+M_{66}+M_{13}\pm[(M_{55}-M_{66}+M_{13})^2+8M_{12}^2]^{1/2}\},$$

$$\omega=-[M_{55}-M_{13}]. \tag{12}$$

The last three eigenvalues are negative, and the actual spin excitation energies are obtained by reversing their signs, which we label by ω_k with $k=5$–7 in ascending order. All seven energy levels hover around the anisotropy energy $2KS$, with the total spread measured by the J_m's. The dispersion of the levels are determined by J_4 through J_6, as indicated by the form of the off-diagonal matrix elements in Eq. (9). Since the J_m's decrease very rapidly for increasing m, the levels are only weakly dispersive.

Direct diagonalization of the 7×7 matrix confirms this picture. In Fig. 1 we show the results of such a calculation using the exchange parameters slightly modified from those estimated in Ref. 6. Our choice of the exchange parameters are $2SJ_m=0.291$, -0.112, -0.128, -0.05, -0.10 meV for $m=1$, 5, and 0 for higher m's. The anisotropy energy parameter $2KS=7.85$ meV was chosen, for reasons to be discussed later. So far the experiments have not resolved the individual levels.

The eigenvectors all have seven components. We write $A_{kn}(q)$ as the nth component of the eigenvector for the eigenvalue $\pm\omega_k$. The four eigenvectors for $k=1$–4 have four major components as given in Eq. (10) and three minor components, while those for $k=5$–7 have three major components as given in Eq. (11) and four minor components. The physical significance of the eigenvectors will be discussed in the next section.

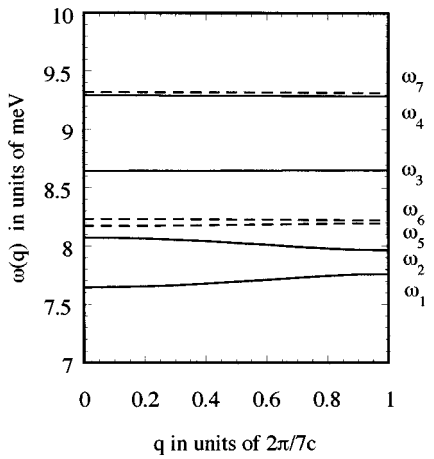

FIG. 1. The calculated spin excitation spectrum of Tm in the ferrimagnetic state. The solid lines are local modes in the spin-up sublattice, and the dotted lines are modes in the spin-down sublattice.

III. NEUTRON SCATTERING CROSS SECTION

The neutron scattering cross section of the kth branch of spin excitation is given by

$$S_k(q,E)\propto S_k(q)\,\delta(E-\omega_k), \tag{13}$$

where

$$S_k(q)=\frac{1}{7}\left|\sum_{n=1}^{7}A_{kn}(q)e^{iqnc/2}\right|^2. \tag{14}$$

The right-hand side of Eq. (14) accounts for the interference effect of the seven spins in a unit cell. The function $S_k(q)$ is periodic in q with the full period of $4\pi/c$, although the terms $A_{kn}(q)$ have the period of $Q=4\pi/7c$. In Fig. 2 we plot $S_k(q)$ in the extended zone scheme. The scattering contributions of all spin-wave branches show strong q dependence, which arises from the symmetry of the eigenvectors. For example, at $q=0$ the eigenvector for the state $k=2$ is nodeless. We represent it symbolically by $(+,+,+,+,+,+,+)$. The Fourier transform of a nodeless function is maximum at $q=0$ and decreases steadily for increasing q, which describes $S_2(q)$ in the top panel of Fig. 2. Similarly, the state $k=4$ has the symmetry symbolized by $(+,-,+,-,-,0,+)$. The corresponding $S_4(q)$ is zero at $q=0$ and increases to a maximum at $q=2\pi/c$. The rise and fall of the other $S_k(q)$'s can be understood in the same way. The patterns are not sensitive to the values of J_m's.

In the experiments the spin-wave levels are not fully resolved, and we simulate this by replacing the δ function in Eq. (13) with a Gaussian. Then the observed neutron scattering cross section can be written as

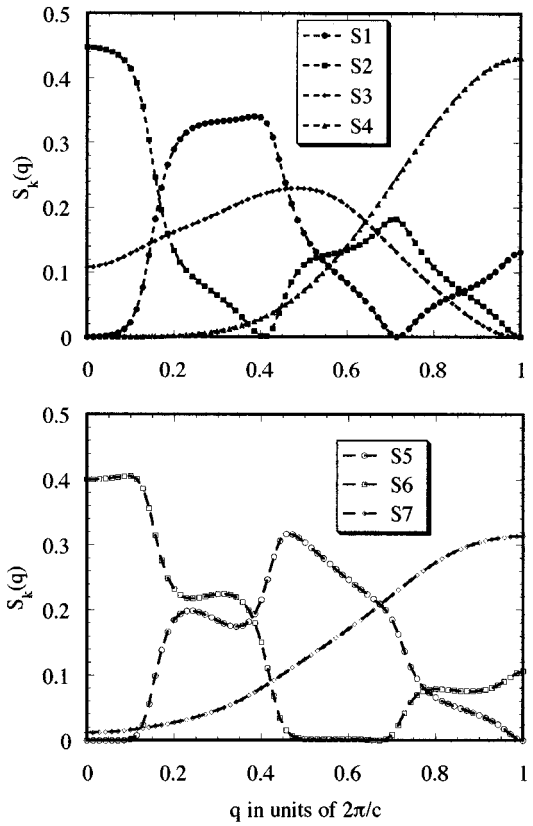

FIG. 2. The contributions of the various spin excitation modes to the neutron scattering cross-section in the extended Brillouin zone of the hcp crystal.

$$S(q,E)=C\sum_{k=1}^{7} S_k(q)e^{-(E-\omega_k)^2/2\Gamma^2}, \tag{15}$$

where Γ parametrizes the resolution width and C is a scale factor. In Fig. 3 we plot three simulated neutron scattering lines. In every case we also plot the three or four lines for the levels which give the largest contributions. The line for $q=0$, the top panel, is matched in peak position and linewidth with the experiment.[8,9] The strongest contributors of this line are the levels $k=2$, 3, and 6. The middle panel shows the line in the middle of the extended zone. Its major contributors are $k=1$, 3, and 5. The lower panel shows a line near the zone boundary, and it comes mainly from the levels $k=2$, 4, 5, and 7. The arrows indicate the measured peak positions. As one can see, the apparent shift of the peak position is due to the wax and wane of the contributions of the individual levels, rather than the shift of the level positions.

In Fig. 4 we compare the calculated and the measured level positions. We used the exchange parameters estimated in Ref. 7 from the magnetization data of Tm, but scaled it down by 15% in order to fit the overall bandwidth. The theory reproduces the observed minimum at about $0.3(2\pi/c)$ for the following physical reason. As shown in Fig. 2, in this range of q the contribution of the $k=2$ level drops sharply and the leading contributor of the scattering strength becomes the $k=1$ level. The dispersion curve dips down because $\omega_1<\omega_2$, which in turn, is due to $J_1>0$ and $J_2<0$. This choice of exchange parameters is required to make certain

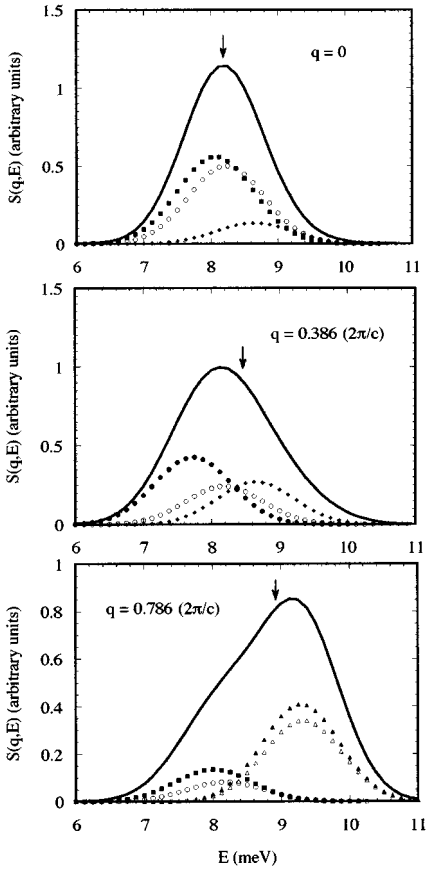

FIG. 3. The simulated neutron scattering lineshape for three q values in the extended zone. Under each curve we show the leading three or four levels which contribute to the total scattering. The component curves are coded according to the legends in Fig. 2. The arrows show the peak positions of the measured lines.

that $\mathcal{J}(\mathbf{q})$ is maximum at $\mathbf{Q}$. Hence the minimum reflects the periodic magnetic structure of Tm.

The theoretical curve is consistently below the data points in the middle of the zone and above the data points in the last third of the zone. It rises sharply near the zone boundary because, as shown in Fig. 2, the scattering contributions of the two highest levels, $k=4$ and 7, rise up and become dominant in this part of the zone. As we discussed before, the q

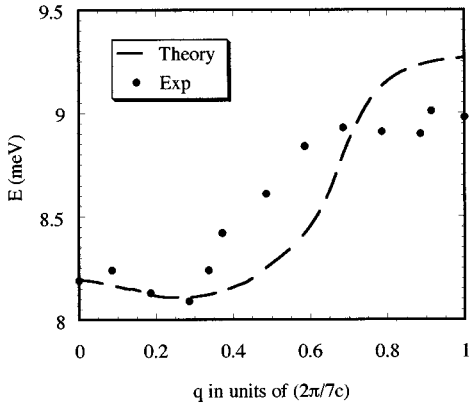

FIG. 4. The calculated apparent dispersion relation of the magnetic excitations versus experimental results for Tm.

dependence of the line intensities depends more strongly on the symmetry of the eigenvectors than the energy parameters. As a result, we have not found it possible to improve the fit by adjusting the exchange parameters. It is gratifying, however, that the largest discrepancy between theoretical and experimental peak positions, about 0.4 meV, is only 25% of the full width at half maximum of the measured lines.

IV. FORMULATION IN THE MOMENTUM SPACE

In this section we will outline an alternative way to formulate the spin excitation problem in the momentum space. The advantage of this method is that the neutron scattering calculation can be done more directly. The hcp structure of the crystal causes some complication because there are two inequivalent sublattices. On the other hand, if we limit our interest to spin excitations propagating along the c axis, the inequivalence the two sublattices is inconsequential. Accordingly, we can define the Fourier transform of the spin operators by

$$\mathbf{S}_q = N^{-1/2}\sum_i \mathbf{S}_i e^{i\mathbf{q}\cdot\mathbf{R}_i}, \tag{16}$$

where $\mathbf{q}=(0,0,q)$. The truncated Hamiltonian for the dynamics of only these modes is

$$H' = -\sum_q \mathcal{J}(q)\mathbf{S}_q\cdot\mathbf{S}_{-q} - K\sum_q S_q^z S_{-q}^z. \tag{17}$$

The operator which excites a spin wave which momentum q is S_q^+, whose equation of motion is

$$\omega S_q^+ = [S_q^+, H'] = N^{-1/2}\sum_{q'} 2[\mathcal{J}(q') - \mathcal{J}(q+q') + K]S_{q+q'}^+ S_{-q'}^z. \tag{18}$$

In the next step we factor out the ordered moments as constants of motion. In the momentum space there are seven components defined by

$$S_m = \frac{1}{7}\sum_{n=1}^{7} \langle S_n^z\rangle e^{imQc/2}, \tag{19}$$

where $Q=4\pi/7c$ and $\langle S_n^z\rangle = S$ or $-S$ depending on whether the site n belongs to the up or the down sublattice. A judicious choice of the magnetic unit cell makes the S_m's all real. We set $\langle S_n^z\rangle = S$ for $n=2,3,4,5$ and $-S$ for $n=1,6,7$ and find

$$S_1 = S_6 = \frac{S}{7}[-1-2\cos\phi + 2\cos 2\phi + 2\cos 3\phi],$$

$$S_2 = S_5 = \frac{S}{7}[-1-2\cos 2\phi + 2\cos 4\phi + 2\cos 6\phi],$$

$$S_3 = S_4 = \frac{S}{7}[-1-2\cos 3\phi + 2\cos 6\phi + 2\cos 9\phi],$$

and

$$S_7 = \frac{S}{7}, \tag{20}$$

where $\phi = 2\pi/7$. The temperature dependence of the S_n's have been measured by Brun *et al.*[5] and calculated by McEwen *et al.*[7] The component S_7, which can also be labeled as S_0, is the ordered ferrimagnetic moment. The equation of motion, Eq. (17), then has the form

$$\omega S_q^+ = 2\sum_n S_n[\mathcal{J}(nQ) - \mathcal{J}(q-nQ) + K]S_{q-nQ}^+. \tag{21}$$

Similarly the equations of motion of S_{q-nQ}^+ can be worked out:

$$\omega S_{q-nQ}^+ = 2\sum_{n'} S_{n'}[\mathcal{J}(n'Q) - \mathcal{J}(q-\{n+n'\}Q) + K]S_{q-(n+n')Q}^+. \tag{22}$$

We define a column vector $\tilde{B}(q)$ whose components are S_{q-nQ}^+ for $n=0$ to 6. The energy level problem again reduces to an eigenvalue problem involving a 7×7 matrix $\tilde{L}(q)$:

$$\omega\tilde{B}(q) = \tilde{L}(q)\tilde{B}(q). \tag{23}$$

The elements of $\tilde{L}(q)$ are

$$L_{nn'}(q) = 2S_{n-n'}[\mathcal{J}(q-\{n-1\}Q) - \mathcal{J}(q-\{n'-1\}Q) + K]. \tag{24}$$

In case $n-n'\leq 0$, the quantity $S_{n-n'}$ is understood to be $S_{n-n'+7}$. The resulting energy levels are identical to those found earlier in Sec. II.

The real advantage of this formalism is that the eigenvectors are directly related to the neutron scattering amplitude. For every energy level k, the seven components of the eigenvector $\tilde{B}(q)$ are the scattering amplitudes in the seven magnetic superzones. Once the components are properly identified with their respective superzone and the q branches folded out, the scattering cross sections $S_k(q)$ are calculated directly by taking the absolute value square of the components. Since error tends to accumulate in any matrix diagonalization procedure, the real space approach, which requires a Fourier analysis of the eigenvectors, is prone to noise. In the momentum space approach, the Fourier transformation is done analytically at the very beginning, thus avoiding a potentially annoying problem.

ACKNOWLEDGMENTS

The author is indebted to Dr. J. F. Cooke, Dr. J. A. Fernandez-Baca, and Dr. R. M. Nicklow for suggesting this investigation and for helpful discussions. He would also like to thank Professor R. C. Dynes and Professor L. J. Sham for their hospitality. A part of this work was done when the author was at the Oak Ridge National Laboratory, supported by the Division of Materials Sciences, U.S. Department of Energy under Contract No. W-7405-eng-26 with the Martin Marietta Energy Systems, Inc.

[1] W. C. Koehler, in *Magnetic Properties of Rare Earth Metals*, edited by R. J. Elliott (Plenum, London and New York, 1972), Chap. 3.

[2] A. R. Mackintosh and H. Bjerrum Møller, in *Magnetic Properties of Rare Earth Metals*, edited by R. J. Elliott (Plenum, London and New York, 1972), Chap. 5.

[3] S. K. Sinha, in *Handbook on the Physics and Chemistry of Rare Earths*, edited by K. A. Gschneidner, Jr. and L. Eyring (North-Holland, Amsterdam, 1978), Vol. I, Chap. 5.

[4] J. Jensen and A. R. Mackintosh, *Rare Earth Magnetism: Structures and Excitations* (Oxford University Press, Oxford, 1991).

[5] T. O. Brun, S. K. Sinha, N. Wakabayashi, G. H. Lander, L. R. Edwards, and F. H. Spedding, Phys. Rev. B **1**, 1251 (1970).

[6] K. A. McEwen and U. Steigenberger, J. Phys. (Paris) Colloq. **49**, C8-335 (1988).

[7] K. A. McEwen, U. Steigenberger, and J. Jensen, Phys. Rev. B **43**, 3298 (1990).

[8] J. A. Fernandez-Baca, R. M. Nicklow, and J. J. Rhyne, J. Appl. Phys. **67**, 5283 (1990).

[9] J. A. Fernandez-Baca, R. M. Nicklow, Z. Tun, and J. J. Rhyne, Phys. Rev. B **43**, 3188 (1991).

[10] U. Steigenberger, K. A. McEwen, J. L. Martinez, and J. Jensen, Physica B **180&181**, 158 (1992); K. A. McEwen, U. Steigenberger, L. Weiss, T. Zeiske, and J. Jensen, J. Magn. Magn. Mater. **140-144**, 767 (1995); R. M. Nicklow and N. Wakabayashi, Phys. Rev. B **51**, 12 425 (1995).

[11] P. Touborg, Phys. Rev. B **16**, 1201 (1977).

[12] T. Nishikubo and T. Nagamiya, J. Phys. Soc. Jpn. **20**, 808 (1965).